POTENTIAL IMPACTS OF METALS ON THE ARIES AND MURES RIVER SYSTEM FOLLOWING ACCIDENTAL TMF SPILLS

By

Professor Paul Whitehead

Oxford Centre for Water research

Oxford University

June 2009

METAL SIMULATIONS DURING A POTENTIAL TMF SPILL

The water in the TMF will contain metals of varying concentration and this has been discussed in the Project EIA reports and one aspect of the project that is important is the potential impact of these metals on the rivers downstream in the event of a TMF spill. Table 1 shows a list of the key metals and compares the TMF concentrations against the surface water standards. As can be seen in the Table, most of the metals are below the standards and this is illustrated by the third column in the Table. Only sulphate, calcium , arsenic and molybdenum are above the standard. (Cyanide has been extensively evaluated and is reported elsewhere).

Table 1 Metal Standards and Predicted Concentrations in the TMF

	Romanian surface water standard mg/l	TMF concentration mg/l	Multiples of Standard
Sulphate	600	2562	4.3
Cyanide Total	0.1	3.2	32.0
Arsenic	0.1	0.2	2.0
Calcium	300.6	594	2.0
Lead	0.2	0.1	0.5
Cadmium	0.2	0.1	0.5
Cromium	1	0.2	0.2
Iron Total	5	0.9	0.2
Copper	0.1	0.1	1.0
Nickel	0.5	0.3	0.6
Zinc	0.5	0.2	0.4
Mercury	0.05	0.01	0.2
Molybdenum	0.1	0.4	4.0
Manganese	1	0.5	0.5
Magnesium	100	9.4	0.1
Cobalt	1	0.5	0.5

In order to assess the impacts of metal release in the event of a TMF failure, a simulation of the 4 metals that exceed the standards has been undertaken. The model used has been developed by Professor Steve Chapra and has already been applied to the simulatate cyanide transport down the river system. A brief description of the model is given in appendix 1 and a full description of the model and its application to the Aries and Mures River System is given by in the Annex reprort and by Chapra and Whitehead (2009).

The Chapra Dispersion model has been used to simulate the metal release from the TMF during a pollution event. The event assumes a total discharge of 26000 cubic metres of flow with the TMF concentrations of 0.2 mg/l of arsenic (As), 0.4 mg/l of Molybdenum (Mo), 2562 mg/l of sulphate and 594mg/l of calcium. These are the maximum concentrations expected in the TMF prior to any potential TMF failure. It is also assumes that a worse case situation downstream whereby that there is no decay or loss of metal by precipitation or sedimentation. It is also assumed that there are two extreme flow condition; firstly when the river flows are low such as in a summer drought or in a winter low flow period and secondly when the river is in spate at high flow conditions. The river system has been set up in the model to simulated the full 595 kms of river from The TMF at Rosia down to the Hungarian border. A full description of all the river ststem set up is given in previous reports (Whitehead, 2007) and in Whtehead et al (2009).

Arsenic Simulation

The simulation results using the Chapra model are given high flow conditions in Figure 1 and Table 1, and the low flow simulation results are given in Figure 2 and Table 2. The results reveal that during high flow conditions there is massive dilution and the pulse of metal rich water rapidly becomes diluted and immediately fall below the Water Standard concentration of 0.1 mg/l. The simulation shows the dispersion effects coupled with the dilution effects as tributuaries join the main river system. The worse case situation is considered here in that it is assumed that there is no precipitation of the metal or sedimentation and that all the metal is held suspended or dissolved in the water column. In the case of the extreme low flow conditions, as shown in Figure 2 and Table 2, the concentrations also fall away rapidly and the dispersion and dilution have a significant effect over the 22 days of travel time down the river system. Again the concentrations fall to well below the Water Standard.

Figure 1 Simulated Arsenic (As) concentrations at key locations along the river system under high flow conditions following the simulated pollution spill

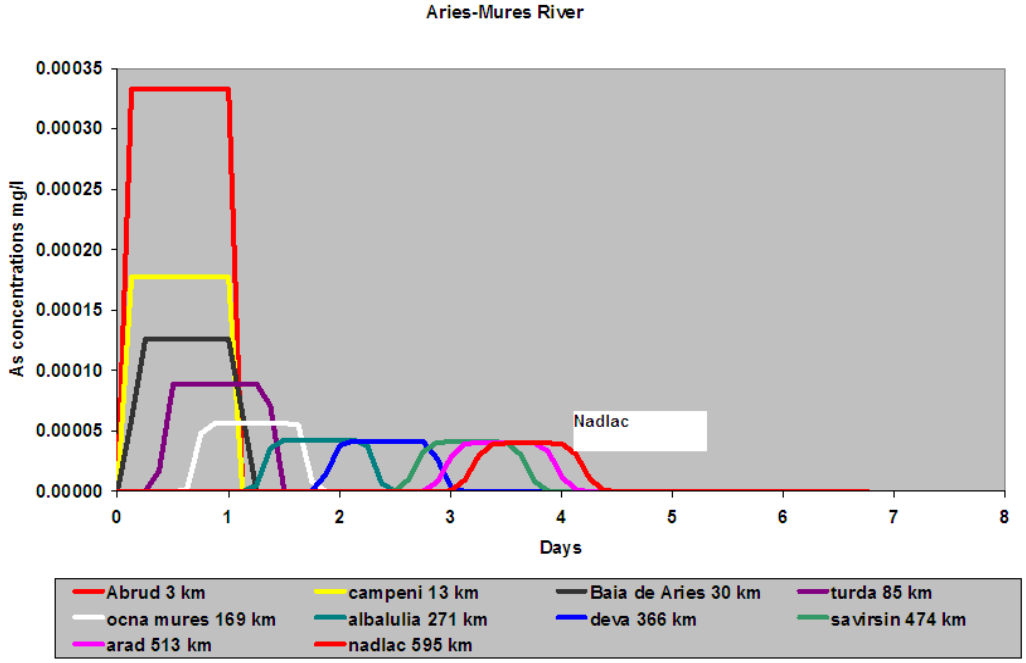

Table 1 Simulated Arsenic (As) concentrations at key locations along the river system under high flow conditions following the simulated pollution spill

Station	Time days	As concentration mg/l
Abrud	0.132	0.00036
campeni	1.012	0.00019
Baia de Aries	1.038	0.00013
turda	1.162	0.00009
ocna mures	1.316	0.00006
albalulia	1.716	0.00004
deva	2.296	0.00004
savirsin	3.121	0.00004
arad	3.413	0.00004
nadlac	3.665	0.00004

Figure 2 Simulated Arsenic (As) concentrations at key locations along the river system under low flow conditions following the simulated pollution spill

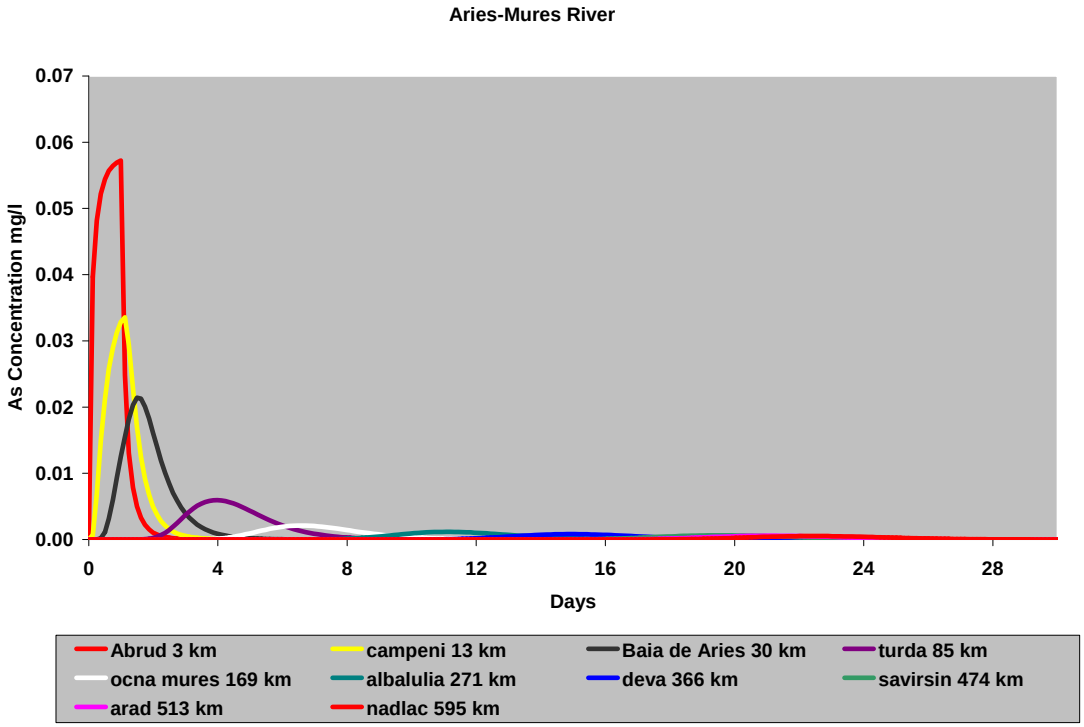

Table 2 Simulated Arsenic (As) concentrations at key locations along the river system under low flow conditions following the simulated pollution spill

Station	Time days	As Peak Concentration mg/l
Abrud	1.002	0.06773
campeni	1.080	0.03634
Baia de Aries	1.502	0.02242
turda	3.922	0.00712
ocna mures	6.561	0.00245
albalulia	11.062	0.00126
deva	14.885	0.00086
savirsin	19.503	0.00066
arad	21.074	0.00059
nadlac	22.404	0.00054

Molybdenum Simulation

In the case of molybdenum, the simulation results are similar to the arsenic results, as shown in Figure 3 and Table 3, for the high flow condition, and in Figure 4 and Table 4, for the low flow condition. Again during high flow conditions there is massive dilution and the pulse of metal rich water rapidly becomes diluted and immediately fall below the Water Standard concentration of 0.1 mg/l. In the case of the low flow conditions, as shown in Figure 4 and Table 4, the concentrations also fall away rapidly and the concentration fall well below the Water Standard.

Figure 3 Simulated Molybdenum (Mo) concentrations at key locations along the river system under high flow conditions following the simulated pollution spill

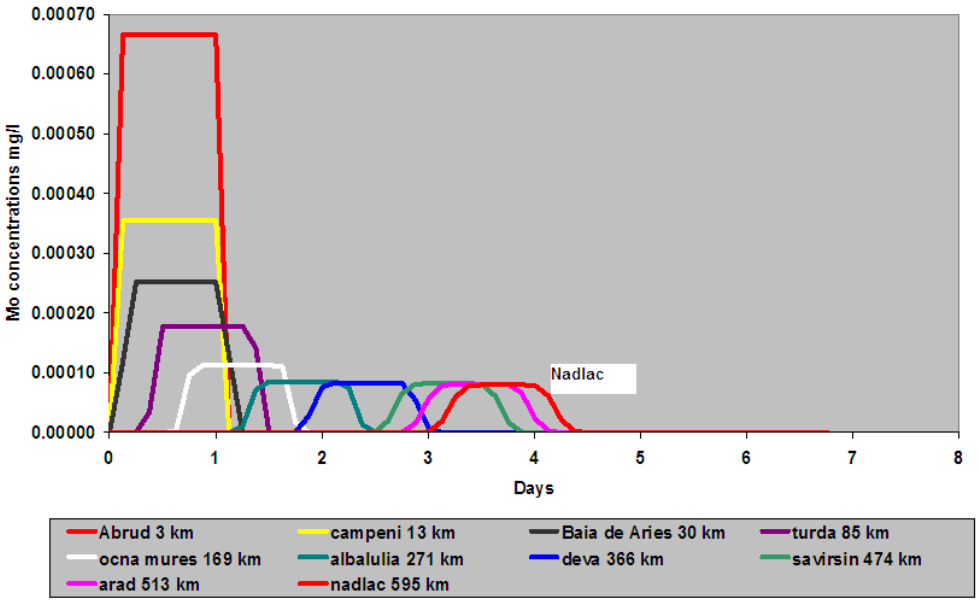

Table 3 Simulated Molybdenum (Mo) concentrations at key locations along the river system under high flow conditions following the simulated pollution spill

Station	Time days	Mo concentration mg/l
Abrud	0.132	0.00072
campeni	1.012	0.00037
Baia de Aries	1.038	0.00026
turda	1.162	0.00019
ocna mures	1.316	0.00012
albalulia	1.716	0.00009
deva	2.296	0.00008
savirsin	3.121	0.00008
arad	3.413	0.00008
nadlac	3.665	0.00008

Figure 4 Simulated Molybdenum (Mo) concentrations at key locations along the river system under low flow conditions following the simulated pollution spill

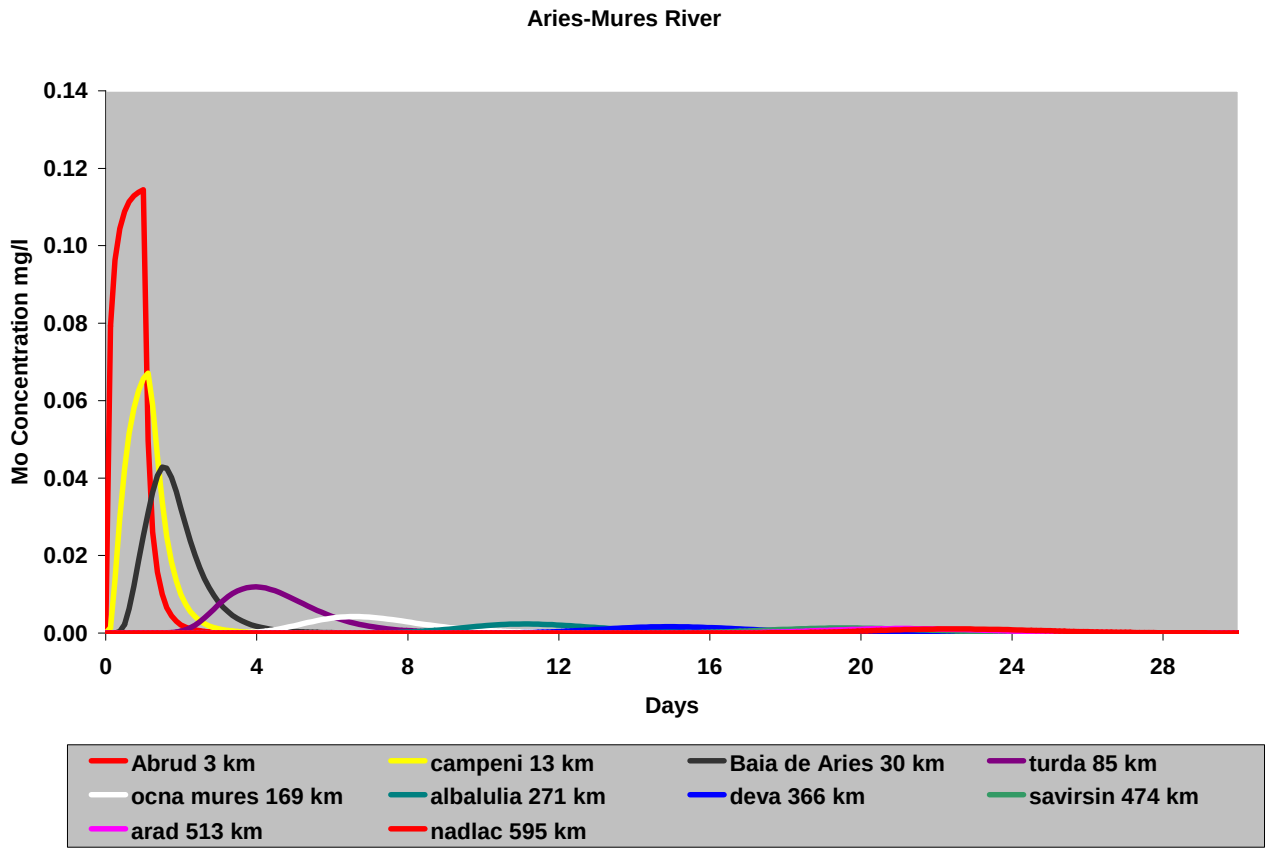

Table 4 Simulated Molybdenum (Mo) concentrations at key locations along the river system under low flow conditions following the simulated pollution spill

Station	Time days	Mo Peak Concentration mg/l
Abrud	1.003	0.135
campeni	1.080	0.073
Baia de Aries	1.502	0.045
turda	3.923	0.014
ocna mures	6.561	0.005
albalulia	11.062	0.003
Deva	14.886	0.002
savirsin	19.504	0.001
arad	21.074	0.001
nadlac	22.404	0.001

Sulphate Simulation

In the case of sulphate, the simulation results are similar to the other metal simulations with reduced concentrations for both high flow and low flow conditions. as shown in Figures 5 and 6 and in Tables 5 and 6. During high flow conditions the dilution reduces the pulse of sulphate rich water rapidly to below the Water Standard concentration of 600mg/l. In the case of the low flow conditions, as shown in Figure 6 and Table 6, the concentrations also fall away rapidly to well below the Water Standard.

Figure 5 Simulated Sulphate concentrations at key locations along the river system under high flow conditions following the simulated pollution spill

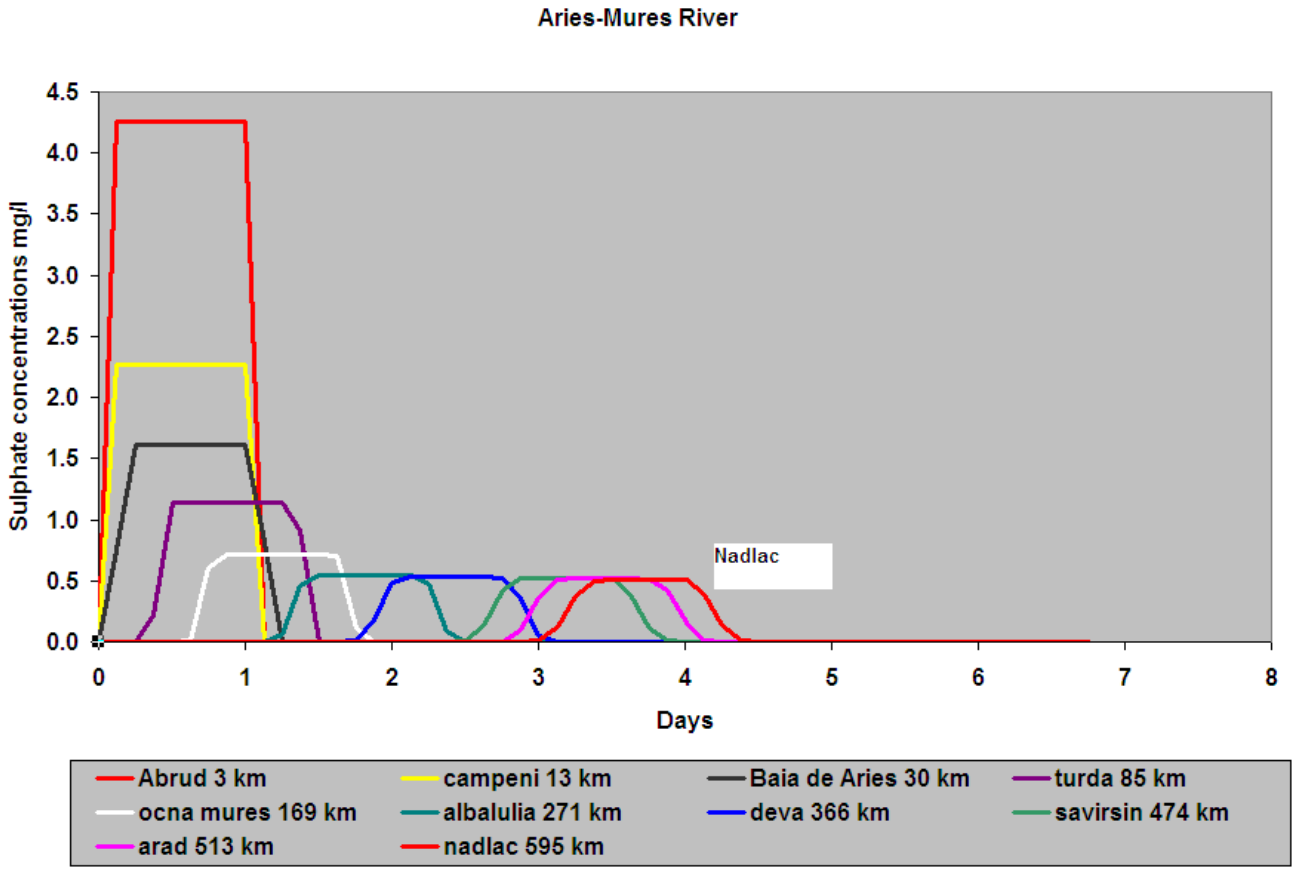

Table 5 Simulated peak sulphate concentrations at key locations along the river system under high flow conditions following the simulated pollution spill

Station	Time days	Sulphate Peak Concentration mg/l
Abrud	0.136	4.30
campeni	0.223	2.38
Baia de Aries	1.039	1.68
turda	1.162	1.19
ocna mures	1.318	0.75
albalulia	1.716	0.55
deva	2.296	0.53
savirsin	3.121	0.53
arad	3.413	0.52
nadlac	3.665	0.51

Figure 6 Simulated Sulphate concentrations at key locations along the river system under low flow conditions following the simulated pollution spill

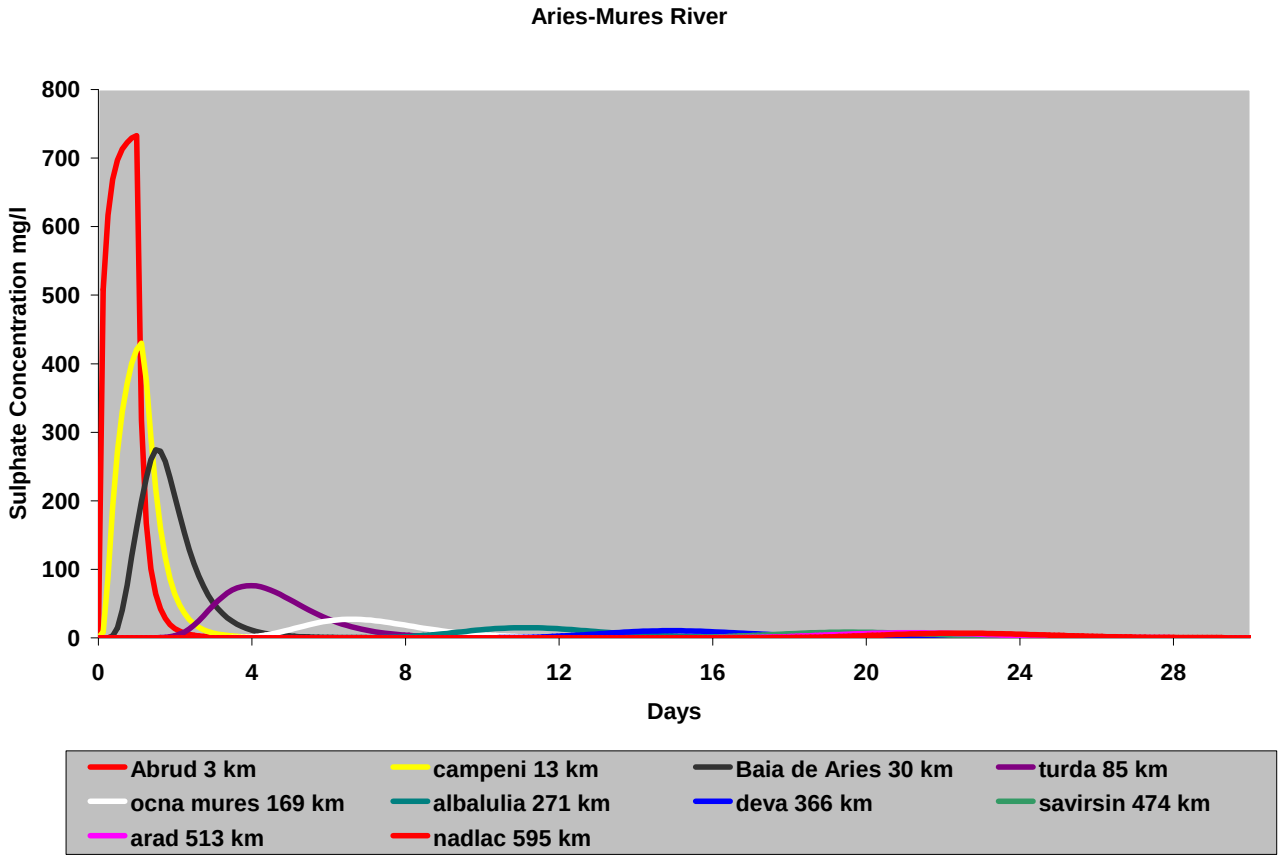

Table 6 Simulated peak sulphate concentrations at key locations along the river system under low flow conditions following the simulated pollution spill

Station	Time days	Sulphate Peak Concentration mg/l
Abrud	1.0	750.6
campeni	1.1	465.5
Baia de Aries	1.5	287.2
turda	3.9	91.2
ocna mures	6.6	31.4
albalulia	11.1	16.1
deva	14.9	11.0
savirsin	19.5	8.5
arad	21.1	7.5
nadlac	22.4	6.9

Calcium Simulation

In the case of calcium, the simulation results are similar to the sulphate simulations with reduced concentrations for both high flow and low flow conditions. as shown in Figures 7 and 8 and in Tables 7 and 8. During high flow conditions the dilution and dispersion rapidly reduce the pulse of calcium to well below the Water Standard concentration of 300 mg/l. In the case of the low flow conditions, as shown in Figure 8 and Table 8, the concentrations also fall away rapidly to concentrations significantly below the Water Standard.

Figure 7 Simulated calcium concentrations at key locations along the river system under high flow conditions following the simulated pollution spill

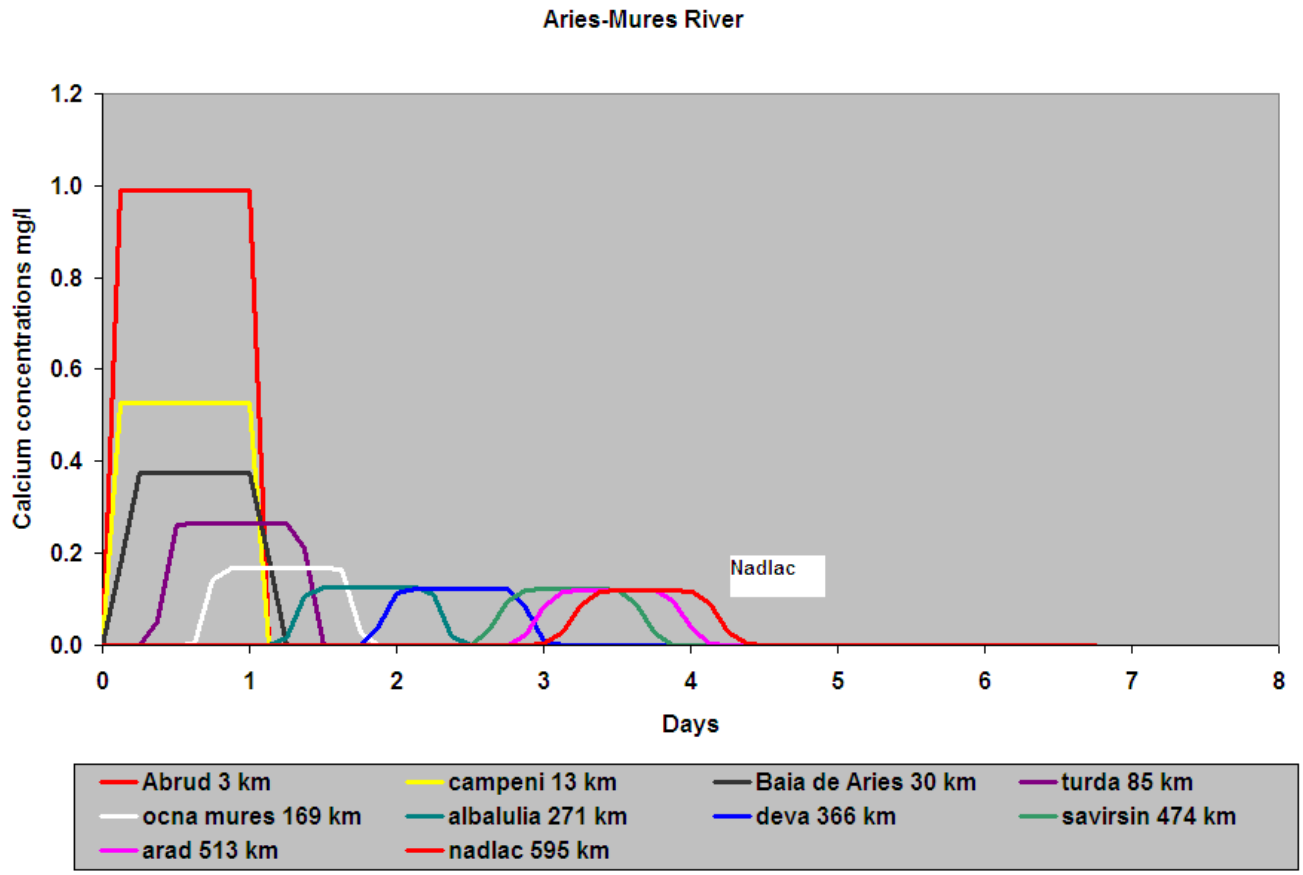

Table 7 Simulated peak cacium concentrations at key locations along the river system under high flow conditions following the simulated pollution spill

Station	Time days	Calciume Peak Concentration mg/l
Abrud	0.136	1.00
campeni	0.223	0.55
Baia de Aries	1.039	0.39
turda	1.162	0.28
ocna mures	1.318	0.17
albalulia	1.716	0.13
deva	2.296	0.12
savirsin	3.121	0.12
arad	3.413	0.12
nadlac	3.665	0.12

Figure 8 Simulated calcium concentrations at key locations along the river system under low flow conditions following the simulated pollution spill

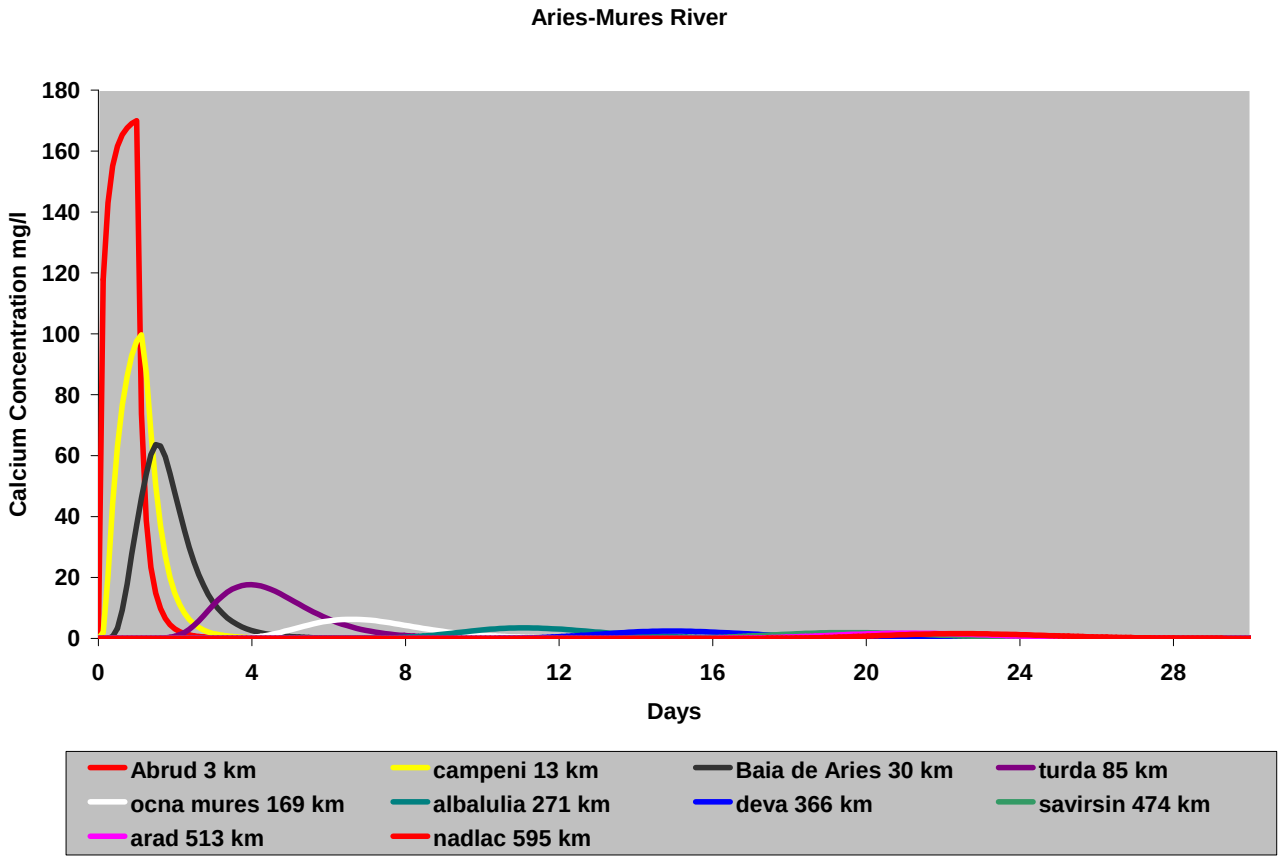

Table 8 Simulated peak calcium concentrations at key locations along the river system under low flow conditions following the simulated pollution spill

Station	Time days	Calcium Peak Concentration mg/l
Abrud	1.0	171.1
campeni	1.1	107.9
Baia de Aries	1.5	66.6
turda	3.9	21.1
ocna mures	6.6	7.3
albalulia	11.1	3.7
deva	14.9	2.6
savirsin	19.5	2.0
arad	21.1	1.8
nadlac	22.4	1.6

CONCLUSIONS

This simulation study has illustrated that metal releases in the event of a TMF failure will fall rapidly to below the Water Standards due to the dilution and dispersion processes operating down the river system.

APPENDIX 1 DISPERSION MODELLING OF POLLUTANT SPILLS

A new model has been developed to numerically simulate the transport and fate of a river contaminant spill. The model is based on the classical dispersion equation (Fischer 1968) but also incorporates the dilution effects of tributaries joining the main river as well as any chemical decay processes occurring in the river system. The model assumes that lateral and vertical gradients are minimal and that the contaminant can decay with first-order kinetics. The general nature of this model is particularly useful as it would be possible to apply the model to any pollutant that has first-order chemical decay or kinetics and almost any river system which is subject to lateral inflows of water that give rise to the dilution effect. The model could therefore be used for radioactive discharges, pesticides, E. coli and any pollutant that can be approximately represented as a simple chemical decay.

In river systems, where there is significant turbulence and mixing, the loss of material by sedimentation or chemical decay can be represented by first-order kinetics dependent on temperature, concentration and river residence time. This kinetic approach to modelling metals and pollutants has been used successfully in the Wheal Jane Mine study by Whitehead *et al*. (2005b) and this is the approach adopted for the modelling of the metals in the current study.

The new model described below has been applied to the Aries and Mures River Systems in Romania, as shown in figures 1 and 2 and a full description of the model is given in the annex report and by Chapra and Whitehead (2009). The river set up and reach structure is also given both in the annex report and in Whitehead et al (2009)

Segmentation

In order to derive a numerical solution the river is divided into a series of reaches, as shown in Figure 3. These reaches represent river segments that have constant hydrogeometric characteristics but the reaches can be of different lengths. The reaches themselves are further divided into a series of equal length computational elements. The elements represent the fundamental units for which water and mass balances are written and solved.

In summary, the nomenclature used to describe the way in which the spill model organizes river topology is as follows.

- Reach: a length of river with constant hydraulic characteristics.
- Element: the model's fundamental computational unit which consists of an equal length subdivision of a reach.

Initial flow balance

A steady-state flow balance is implemented for each model element. For the first element in a reach, the budget is written as (see Figure 4):

$$Q_i = Q_{i-1} + Q_{\text{in},i} \qquad (1)$$

where Q_i = outflow from element i into the downstream element $i + 1$ ($m^3 s^{-1}$), Q_{i-1} = inflow from the upstream element $i - 1$ ($m^3 s^{-1}$), and $Q_{\text{in},i}$ is the incremental inflow into the element from point and non-point sources along the length of the reach ($m^3 s^{-1}$). Thus, the downstream outflow of the first element is simply the sum of the inflow from upstream and the incremental flow. For the other elements of the reach $Q_{\text{in},i} = 0$ and, therefore, outflow equals inflow i.e. $Q_i = Q_{i-1}$.

Depth, velocity and other hydraulic parameters

Once the outflow for each element is computed, the depth H_i (m) and velocity U_i ($m s^{-1}$), are calculated in one of two ways: rating curves and the Manning equation.

Rating curves. Rating curves in the form of power equations are used to relate mean velocity and depth to flow for each element:

$$U_i = aQ_i^b \quad (2)$$

$$H_i = \alpha Q_i^\beta \quad (3)$$

where U_i = the mean velocity across the downstream interface of element i (m s^{-1}), H_i = the average depth of element i (m) and a, b, α and β are empirical coefficients that are determined from velocity–discharge and stage–discharge rating curves, respectively. Note that the sum of b and β must be less than or equal to 1. If this is not the case, the width will decrease with increasing flow. If their sum equals 1, the channel is rectangular.

After the velocity and depth of an element are computed with Equations (2) and (3), they can be used to compute other required hydrogeometric characteristics. For example, the velocity can be substituted into the continuity equation ($Q_i = U_i A_{c,i}$) to determine the element's cross-sectional area (m^2):

$$A_{c,i} = \frac{Q_i}{U_i}. \quad (4)$$

The area can be directly related to flow by substituting Equation (2) into Equation (4) to give

$$A_{c,i} = \frac{Q_i}{aQ_i^b} = \frac{1}{a} Q_i^{1-b}. \quad (5)$$

The element's mean width B (m), wetted perimeter P (m) and volume V (m^3) follow

$$B_i = \frac{A_{c,i}}{H_i} \quad (6)$$

$$P_i = B_i + 2H_i \quad (7)$$

$$V_i = B_i H_i \Delta x_i \quad (8)$$

where Δx_i = the element length (m).

Besides computing the hydrogeometric characteristics as a function of flow, the rating curves can also be employed to perform the inverse calculation. That is, given volume, they can also be used to compute flow, depth, velocity, area, width and wetted perimeter. Because Δx is known, we first determine the cross-sectional area as:

$$A_{c,i} = \frac{V_i}{\Delta x_i} \quad (9)$$

Flow can then be evaluated by solving Equation (5) for

$$Q_i = a^{1/(1-b)} A_c^{1/(1-b)}. \quad (10)$$

Once flow is known, Equations (2), (3), (6) and (7) can be then employed to compute U_i, H_i, B_i, and P_i.

Manning equation

Each element in a particular reach is idealized as a trapezoidal channel (Figure 5). For such channels, the Manning equation can be used to express the relationship between flow and depth as

$$Q_i = \frac{S_{0,i}^{1/2}}{n_i} \frac{A_{c,i}^{5/3}}{P_i^{2/3}} \quad (11)$$

where $S_{0,i}$ = bottom slope (m m^{-1}), n_i = the Manning roughness coefficient, $A_{c,i}$ = the cross-sectional area (m^2) and P_i = the wetted perimeter (m).

The cross-sectional area and wetted perimeter are computed as

$$A_{c,i} = \left(B_{0,i} + s_i H_i\right) H_i \qquad (12)$$

$$P_i = B_{0,i} + 2H_i\sqrt{s_i^2 + 1} \qquad (13)$$

where $B_{0,i}$ = bottom width (m) and s_i = the side slope as shown in Figure 5 (m m^{-1}). Substituting Equations (12) and (13) into (11) gives

$$Q_i = \frac{1}{n_i}\frac{\left[\left(B_{0,i} + s_i H_i\right) H_i\right]^{5/3}}{\left[B_{0,i} + 2H_i\sqrt{s_i^2 + 1}\right]^{2/3}} S_{0,i}^{1/2}. \qquad (14)$$

Given values for Q, B_0, S_0, n and s, Equation (14) is a nonlinear equation with one unknown H which can be reformulated as

$$f(H_i) = \frac{1}{n_i}\frac{\left[\left(B_{0,i} + s_i H_i\right) H_i\right]^{5/3}}{\left[B_{0,i} + 2H_i\sqrt{s_i^2 + 1}\right]^{2/3}} S_{0,i}^{1/2} - Q_i. \qquad (15)$$

The root (i.e. the value of depth that makes this equation zero) is the reach depth. It can be shown that the root can be determined efficiently by successive substitution (Chapra & Canale 2006) using the iterative formula:

$$H_{i,k} = \frac{(Q_i n_i)^{3/5}\left(B_{0,i} + 2H_{i,k-1}\sqrt{s_i^2 + 1}\right)^{2/5}}{S_{0,i}^{3/10}\left[B_{0,i} + s_i H_{i,k-1}\right]} \qquad (16)$$

where k = 1, 2, …, n, where n = the number of iterations. If an initial guess of $H_{i,0} = 0$ is employed, this approach is rapidly convergent for all natural channels (Chapra & Canale 2006). The method is terminated when the estimated error falls below a specified value of 0.001%. The estimated error is calculated as

$$\varepsilon_{a,i} = \left|\frac{H_{i,k+1} - H_{i,k}}{H_{i,k+1}}\right| \times 100\% \qquad (17)$$

Once the depth is known, the cross-sectional area and wetted perimeter are computed with Equations (12) and (13), and the velocity can be determined from the continuity equation:

$$U_i = \frac{Q_i}{A_{c,i}} \qquad (18)$$

The average element width, B_i (m) is then computed as

$$B_i = \frac{A_{c,i}}{H_i}, \qquad (19)$$

the top width, $B_{1,i}$ (m) as

$$B_{1,i} = B_{0,i} + 2s_i H_i \qquad (20)$$

and the element volume as

$$V_i = B_i H_i \Delta x_i. \qquad (21)$$

As was the case with the rating curves, the Manning approach can also be employed to perform the inverse calculation. If the volume is given, the cross-sectional area can be generated with Equation (9). The depth is determined by reformulating Equation (12) as a quadratic, i.e.

$$s_i H_i^2 + B_{0,i} H_i - A_{c,i} = 0. \qquad (22)$$

The positive root of this equation yields the depth (note that this version of the quadratic formula prevents division by zero for rectangular channels i.e. with $s_i = 0$):

$$H_i = \frac{2A_{c,i}}{B_{0,i} + \sqrt{B_{0,i}^2 + 4s_i A_{c,i}}}. \qquad (23)$$

The average width and flow are computed with Equations (19) and (14), respectively, and the velocity then follows from Equation (18).

Dynamic water balance

After the initial volumes are determined, the software generates a numerical solution of the one-dimensional continuity equation:

$$\frac{\partial A_c}{\partial t} = -\frac{\partial Q}{\partial x} \qquad (24)$$

Equation (24) can be expressed in numerical form by writing a water balance around each element to give

$$\frac{dV_i}{dt} = Q_{i-1} + Q_{i,\text{in}} - Q_i \qquad (25)$$

where Q_i is the outflow which is computed as described previously. Equation (25) is then integrated numerically to obtain the element volumes as a function of time.

Dispersion

Dispersion can either be user-prescribed or computed. In the latter case, based on Rutherford's (1994) assessment, three empirically-derived equations are available to compute the longitudinal dispersion for the downstream boundary between two elements.

According to Fischer *et al*. (1979),

$$E_{p,i} = 0.011 \frac{U_i^2 B_i^2}{H_i U_i^*} \qquad (26)$$

where $E_{p,i}$ = the longitudinal dispersion between elements i and $i + 1$ ($m^2\ s^{-1}$) and U_i = mean velocity of element i ($m\ s^{-1}$), B_i = mean width (m), H_i = depth (m) and U_i^* = shear velocity ($m\ s^{-1}$), which is related to more fundamental characteristics by

$$U_i^* = \sqrt{gH_i S_{0,i}} \qquad (27)$$

where g = acceleration due to gravity (= 9.81 $m\ s^{-2}$) and $S_{0,i}$ = bottom slope ($m\ m^{-1}$).

According to Liu (1977),

$$E_{p,i} = 0.18 \left(\frac{U_i^*}{U_i} \right)^{1.5} \frac{Q_i^2}{U_i^* R_h^3} \qquad (28)$$

where R_h = the hydraulic radius (m), equal to the ratio of the cross-sectional area to the wetted perimeter.

According to McQuivey and Keefer (1974),

$$E_{p,i} = 0.058 \frac{Q_i}{S_i B_i}. \qquad (29)$$

This formulation is limited to systems with Froude numbers ($F = U/\sqrt{gH}$) less than 0.5. If this constraint is exceeded, the software automatically displays an error message and terminates.

Mass balance

The software generates a numerical solution of the one-dimensional advection-dispersion-reaction equation:

$$\frac{\partial c}{\partial t} = -\frac{\partial Uc}{\partial x} + \frac{\partial}{\partial x}\left(E\frac{\partial c}{\partial x}\right) - kc \qquad (30)$$

where c = concentration (mg l^{-1}), t = time (s), U = velocity (m s^{-1}), x = distance (m), E = dispersion (m^2 s^{-1}) and k = first-order decay rate (d^{-1}).

Equation (30) can be expressed in numerical form by writing a mass balance around each element, as shown in Figure 6. In order to account for the non-uniformity, as well as to conserve mass, the fluxes between elements are specified at their upstream and downstream faces to give:

$$\frac{\partial M_i}{\partial t} = \left(UA_c c - EA_c\frac{\partial c}{\partial x}\right)_{i-1,i} - \left(UA_c c - EA_c\frac{\partial c}{\partial x}\right)_{i,i+1} - kV_i c_i \qquad (31)$$

where M_i = the mass of pollutant in element i (g) = $V_i\, c_i$.

Assuming that the concentrations at each interface are equal to the upstream element (i.e. a backward or 'upstream' difference), and using centred differences for the gradients, yields:

$$\frac{dM_i}{dt} = W(t) + Q_{i-1,i}c_{i-1} - Q_{i,i+1}c_i + E_{i-1,i}A_{c,i-1,i}\frac{c_{i-1}-c_i}{\Delta x_{i-1,i}} + E_{i,i+1}A_{c,i,i+1}\frac{c_{i+1}-c_i}{\Delta x_{i,i+1}} - kV_i c_i \quad (32)$$

where $W(t)$ = mass loading rate (g s^{-1}), $Q_{j,k}$ = the flow from element j into element k (m^3 s^{-1}), $E_{j,k}$ = the dispersion between elements j and k (m^2 s^{-1}) and $\Delta x_{j,k}$ = the length between the mid-points of elements j and k (m):

$$\Delta x_{j,k} = \frac{\Delta x_j + \Delta x_k}{2} \qquad (33)$$

where Δx_i = the length of element i (m). This equation can then be written for all the elements and integrated numerically to obtain the solution.

Solution method

Equations (25) and (32) are solved numerically with Euler's method as follows:

1. Determine and save the initial values for all elements.
2. Compute derivatives with Equations (25) and (33).
3. Compute new volumes and masses with Euler's method:

$$V_i(t+\Delta t) = V_i(t) + \frac{dV_i(t)}{dt}\Delta t$$

$$M_i(t+\Delta t) = M_i(t) + \frac{dM_i(t)}{dt}\Delta t$$

4. Compute new outflows for each element as a function of their new volumes.
5. Compute other hydraulic parameters.
6. Compute new concentrations: $c_i = M_i/V_i$.
7. Increment time: $t = t + \Delta t$.
8. Save new values. If $t \geq$ final time, exit to Step 10.
9. Loop back to Step 2.
10. Display results.

In the absence of numerical dispersion, the foregoing hydraulic solution is similar to the kinematic wave. However, because of the use of first-order forward time differencing and backward space differencing, it does exhibit numerical dispersion and hence is more akin to a diffusive wave solution. Techniques such as the Muskingum-Cunge method attempt to mitigate such effects; the solution time-step is selected in order that the numerical dispersion approximates the actual diffusion exhibited by waves subject to gravity effects.

In a similar fashion, the mass solution also generates additional numerical dispersion. As with the hydraulics, a time-step can be chosen in an attempt to match the numerical dispersion to the actual dispersion.

Unfortunately, different time-steps are needed for the hydraulic and mass solutions. Further, because the system being studied has a wide range of flows and velocities, the optimal time-step will vary greatly. The following scheme attempts to minimize the impact of both effects while using a single time-step.

For the mass solution, the total dispersion generated consists of the model dispersion, E_i, along with some additional numerical dispersion, $E_{n,i}$. Since we would like the solution to have the correct physical dispersion (i.e. either user-specified or computed with Equations (26)–(29)) $E_{p,i}$, we therefore desire that

$$E_{p,i} = E_i + E_{n,i}. \quad (34)$$

A Taylor series expansion (Chapra 1997) can be used to relate the numerical dispersion to the space and time-steps as

$$E_{n,i} = 0.5U_i\Delta x_i - 0.5U_i^2\Delta t. \quad (35)$$

Substituting Equation (35) into (34) and rearranging yields

$$E_i = E_{p,i} - 0.5U_i\Delta x_i + 0.5U_i^2\Delta t. \quad (36)$$

Therefore, to achieve accuracy, the dispersion used in the model E_i is automatically set equal to the desired dispersion: $E_{p,i}$ minus the numerical dispersion $E_{n,i}$.

There are two stability constraints. First, a spatial positivity constraint can be formulated as

$$\Delta x_i < \frac{2E_i}{U_i}. \quad (37)$$

This constraint guarantees positive solutions.

In addition, the time-step is constrained according to

$$\Delta t < \frac{\Delta x_i^2}{U_i\Delta x_i + 2E_i + k\Delta x_i^2} \quad (38)$$

where the right-hand side is the element's residence time (s). This is the analogue of the Courant condition for Equation (32). These criteria can be used to develop a solution procedure that maximizes accuracy and guarantees stability as described next. First, the user specifies the maximum desired size of the element length for each reach. Then, Equation (37) is used to determine the maximum permissible size based on the velocity and the dispersion, i.e. using $E_i = E_{p,i}$. If the desired size is greater than the permissible size, the element length is set to the permissible size. Otherwise, the element length is set to the maximum desired size. The resulting element length is then divided into the reach length and the result rounded up in order to determine the number of elements for each reach. Second, Equation (38) is used to determine a maximum allowable time-step for each reach. The minimum of these time-steps is then taken as the computational time-step for the entire system. Finally, this time-step along with the element size is substituted into Equation (35) to compute the numerical dispersion. If it is less than the physical dispersion, Equation (36) is used to compute the dispersion coefficient that should be input to the model.

A full description of the model and its application is given in the annex report and by Chapra and Whitehead (2009). The river set up and reach structure is also given both in the annex report and in Whitehead et al (2009)

FIGURES

Figure 1 | Romania and the location of Roşia Montană

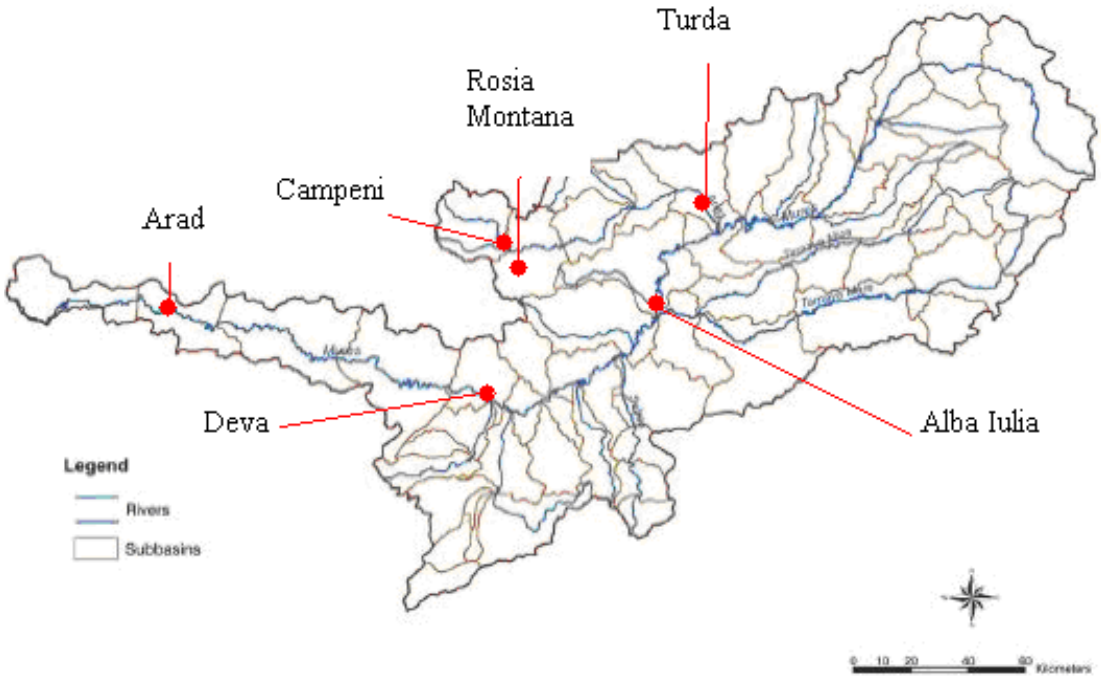

Figure 2 The Mures River basin, key locations and sub-catchments

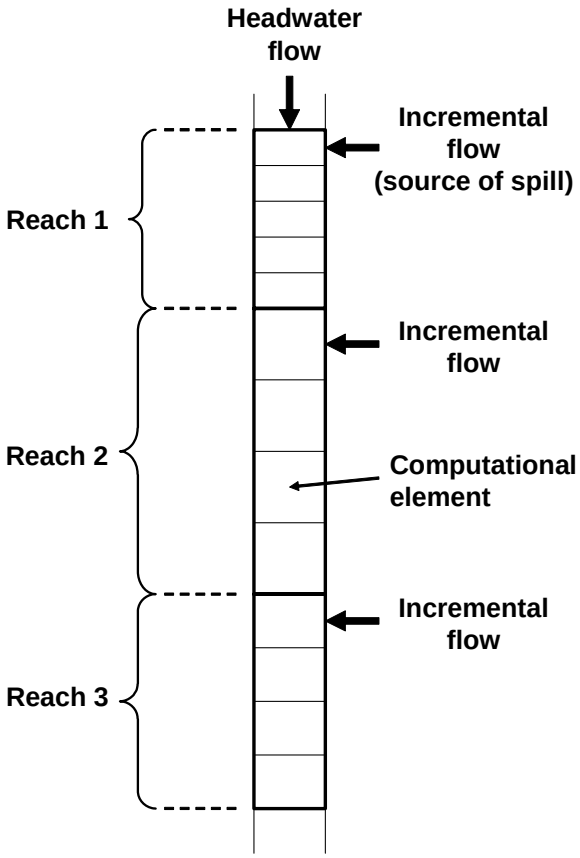

Figure 3 Spill model segmentation scheme showing reaches divided into equal-sized computational elements (the system's external flows are also depicted)

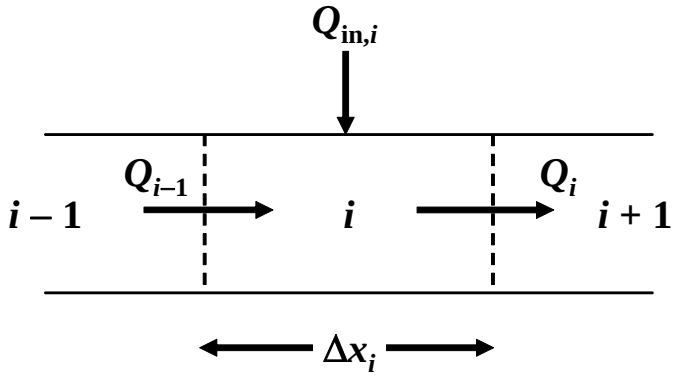

Figure 4 Flow balance for the first element in a reach

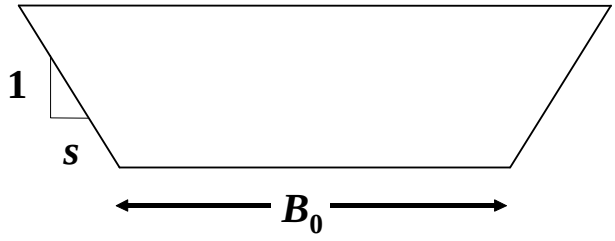

Figure 5 A cross-section of a trapezoidal channel showing the parameters needed to uniquely define the geometry: B_0 = bottom width, s = side slope

Figure 6

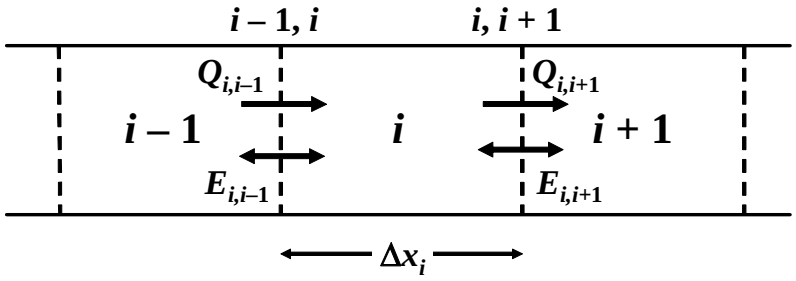

Figure 6 One-dimensional channel divided into a series of elements

REFERENCES

Chapra SC. 1997. *Surface Water-Quality Modeling*. McGraw-Hill, New York.

Chapra SC & Canale RP. 2006. *Numerical Methods for Engineers*. McGraw Hill, New York

Chapra, S. & Whitehead, P. G. 2009 Modelling impacts of pollution in river systems: a new dispersion model and a case study of mine discharges in the Abrud, Aries and Mures River System in Transylvania, Romania. Hydrol. Res. 40(2–3), 306–322.

Fischer HB. 1968. Dispersion Predictions in Natural Streams. *J. San. Engr. Div. ASCE* **94**(SA5), 927–944.

Fischer HB, List EI, Koh RCY, Imberger J & Brooks NH. 1979. *Mixing in Inland and Coastal Waters*. Academic, New York.

Johnson DB & Hallberg KB. 2005. Acid Mine Drainage Options: A review. *Sci. Totl. Env*. **338**, 3–15.

Liu H. 1977. Predicting Dispersion Coefficients in Streams. *J. Envir. Engr. Div. ASCE* **103**(EE1), 59–69.

McQuivey RS & Keefer TN. 1974. Simple Method for Predicting Dispersion in Streams. *J. Environ. Engr. Div. ASCE* **100**(EE4), 997–1011.

Neal C, Whitehead PG, Jeffery H & Neal M. 2005. The Water Quality of the River Carnon, West Cornwall, November 1992 to March 1994: the Impacts of Wheal Jane Discharges. *Sci. Totl. Env*. **338**, 23–41.

Nordstrom DK, Alpers CN, Ptacek CJ & Blowes DW. 2000. Negative pH and extremely acidic mine waters from Iron Mountain, California. *Environmental Science and Technology* **34,** 254–258.

Rutherford JC. 1994. *River Mixing*. Wiley, New York.

Whitehead PG & Prior H. 2005 Bioremediation of Acid Mine Drainage: an Introduction to the Wheal Jane Wetlands Project. *Sci. Totl. Env*. **338**, 15–21.

Whitehead PG, Hall G, Neal C & Prior H. 2005a. Chemical Behaviour of the Wheal Jane Bioremediation System. *Sci. Totl. Env*. **338**, 41–55.

Whitehead PG, Cosby BJ & Prior H. 2005b. The Wheal Jane Wetlands Model for Bioremediation of Acid Mine Drainage. *Sci. Totl. Env*. **338**, 125–135.
Whitehead PG, Butterfield D & Wade A. J. 2009. Simulating Metals and Mine Discharges in River Basins using a new Integrated Catchment Model for metals: Pollution impacts and Restoration strategies in the Aries-Mures river system in Transylvania, Romania *Hydrology Research* . Vol 40(2–3), 323–345